



Enhancing the vibratory roller's ride comfort with semi-active seat suspension embedded by quasi-zero stiffness structure

Tianfeng Ye¹ · Vanliem Nguyen² · Shiming Li²

Received: 27 September 2022 / Revised: 31 December 2022 / Accepted: 23 January 2023 / Published online: 3 February 2023
© The Author(s), under exclusive licence to Springer-Verlag GmbH Germany, part of Springer Nature 2023

Abstract

To enhance the vibratory roller's ride quality, semi-active suspension of the driver's seat embedded by the quasi-zero-stiffness-structure (QZSS) has been proposed and researched. A dynamic model of the vibratory roller is established to evaluate the ride quality of the vehicle and the efficiency of the QZSS added into the semi-active seat suspension under the various operating conditions of the vibratory roller. The experiment with the vibratory roller is also given to verify the accuracy of the mathematical model. Two indexes of the root mean square seat acceleration in the time domain (a_{ws}) and power spectral density (PSD) seat acceleration in the frequency domain are chosen as the objective functions. The study indicates that the vehicle's ride quality with the semi-active seat suspension is better than that of the passive seat suspension, while the vehicle's ride quality with the semi-active seat suspension embedded by the QZSS is remarkably improved in compared to the semi-active seat suspension without the QZSS. Especially, the a_{ws} and maximum PSD of the driver's seat are greatly decreased by 76.0% and 73.4% in comparison with the passive seat suspension, respectively. Consequently, the semi-active seat suspension should be embedded by the QZSS to further improve the vibratory roller's ride quality.

Keywords Vibratory roller · Quasi-zero-stiffness-structure · Semi-active seat suspension · Ride quality

1 Introduction

When the vibratory roller was moving and working on the elastoplastic soil ground, the vertical vibration of the driver's seat and the cab shaking were very high. They greatly affected the driver's ride comfort [1, 2]. Therefore, to improve the vibratory roller's ride comfort, the vehicle cab's rubber mounts were researched and replaced by using hydraulic mounts [3]. Moreover, based on the optimal controllers of the PID-fuzzy controller and optimal fuzzy controller, the cab's semi-active hydraulic mounts of the vibratory roller were then controlled to further improve the driver's ride comfort [3, 4]. The study results showed that the vehicle's ride comfort using the cab's semi-active hydraulic mounts was remarkably improved in comparison with the rubber mounts

and hydraulic mounts without control. However, according to ISO 2631-1 [5], the driver's seat acceleration response was still high, especially under the condition of the vibratory roller working on the elastoplastic soil grounds. Therefore, the driver's seat passive suspension of the vibratory roller needs to be redesigned to improve the driver's ride comfort.

In the suspension systems of the vehicle, cab, and seat, the passive suspension had been replaced by using the semi-active suspension controlled by Neuro control, PID control, Fuzzy control, or Feedback control to improve the vehicle's ride comfort [3, 4, 6–10]. The result indicated that the vehicle's ride comfort was obviously improved in comparison without the control, especially with using the fuzzy controller. However, the control of the driver's seat suspension of the vibratory rollers has not yet been concerned in the existing studies.

Besides, with the seat's passive suspension of the vehicles, a new design of the quasi-zero-stiffness-structure (QZSS) added into the seat's passive suspension to improve the vehicle's ride comfort had been researched and developed [11, 12]. The design parameters of the QZSS were also optimized by the genetic algorithm to enhance its isolation performance [13]. The isolation performance of the QZSS was then tested

✉ Vanliem Nguyen
xuanliem712@gmail.com

¹ School of Electrical and Electronic Information Engineering, Hubei Polytechnic University, Huangshi 435003, China

² Hubei Key Laboratory of Intelligent Conveying Technology and Device, Hubei Polytechnic University, Huangshi 435003, China

to validate the research result [14]. The research results manifested that with the seat’s passive suspension embedded by the QZSS, the vehicle’s ride comfort was strongly ameliorated in comparison without the QZSS. However, in the above studies, the 1-D model of the vehicle dynamic had been only established to assess the isolation performance of the QZSS [11–14] while the actual structure of the vehicles is a 3-D structure. Therefore, the QZSS’s performance had not been fully evaluated yet.

The isolation performance of the QZSS and semi-active suspension for the driver’s seat suspension of the vehicles was researched in the existing studies. However, the application of the QZSS and semi-active suspension on the driver’s seat suspension of off-road vibratory rollers had not been performed yet. Furthermore, a combination of both QZSS and semi-active suspension of the driver’s seat suspension could further ameliorate the vehicle’s ride comfort. However, this problem has not been concerned yet. In addition, in all vibration models of the QZSS and semi-active suspension, the excitation of the rigid road surface was only applied to evaluate their isolation performance. With the vibratory rollers, they mainly move and compress on the elastoplastic soil ground. Therefore, the isolation performance and stability of both QZSS and semi-active suspension of the driver seat could be affected by the excitation of the deformable terrain. However, this problem has not been evaluated yet.

In order to solve the above existing problems, a semi-active suspension added by the QZSS is proposed and studied for the vibratory roller’s seat suspension. A 3-D model of the vibratory roller dynamic is established to assess the vehicle’s ride comfort under the various working conditions of the vibratory roller. The vibratory roller experiment is also performed to ensure the reliability of the mathematical model as well as the calculation results. The reduction of both the weighted root mean square acceleration and power spectral density acceleration of the driver’s seat is chosen as the objective function to evaluate the vibratory roller’s ride comfort.

2 Dynamic models of vibratory roller

2.1 Modeling of the vibratory roller dynamic

To determine the vibration equations of the vibratory roller and assess the driver’s ride comfort, a 3-D vehicle dynamic model with 11 degrees of freedom had been built under the interaction of the wheel/drum and elastoplastic terrain, as shown in Fig. 1. Where, z_δ and m_δ are the displacement and mass of the driver’s seat, cab, front/rear vehicle floor, and drum; θ_ϑ is the rolling angles of cab, front/rear vehicle floor, and drum; ϕ_c and ϕ_{rb} are the cab and rear vehicle floor’s pitching angles; $\{c_{dj}, c_{wj}\}$ and $\{k_{dj}, k_{wj}\}$ are the passive damping coefficients and passive stiffness coefficients

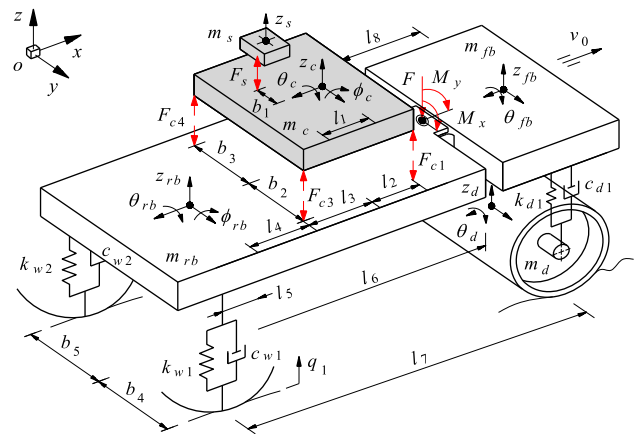


Fig. 1 The 3-D dynamic model of the vibratory roller

of the drum isolations and wheels; F_s is the vertical force response of the driver’s seat suspension; F_{ci} are the vertical force responses of the cab’s isolation systems; q_j are the vibration excitations of the vibratory roller under the wheels; v_0 is the vehicle’s moving velocity; l_{1-8} are the vibratory roller’s distances in the x direction; and b_{1-5} are the vibratory roller’s distances in the y direction; $i = 1-4$; $j = 1-2$; $\delta = s, c, fb, rb, d$; and $\vartheta = c, fb, rb, d$.

In order to reduce the computational complexity of the vibratory roller’s vibration equations, some assumptions are given to overcome some limitations of the model as follows: (1) the displacement of the driver’s seat, cab floor, and front/rear vehicle floor around their equilibrium position are very small; (2) the deformation of the cab’s floor and rear floor of the vibratory roller is also very small; (3) at the swivel joint between the front floor and rear floor of the vehicle body, there are two yawing and rolling motions, other motions are constrained; and (4) assuming that the longitudinal and horizontal impacts are very small and ignored due to the vibrations of the vibratory roller being generated by the wheel/drum and deformable terrain interaction in the vertical direction.

By application of Newton’s second law of motion for the dynamic model of the vibratory roller in Fig. 1, the vibration equations of the vehicle could be written in the matrix form as follows:

$$M\ddot{Z}(t) + C\dot{Z}(t) + KZ(t) = F(t) \tag{1}$$

where M is the mass matrix, C is the damping coefficient matrix, and K is the stiffness coefficient matrix; $\ddot{Z}(t)$ is the acceleration vector, $\dot{Z}(t)$ is the velocity vector, $Z(t)$ is the displacement vector; and $F(t)$ is the vector of the exciting forces of the model, respectively.

The excitation force F_{ci} of the cab isolation, excitation force F_{wj} of the wheels, and excitation force F_{dj} of the drum

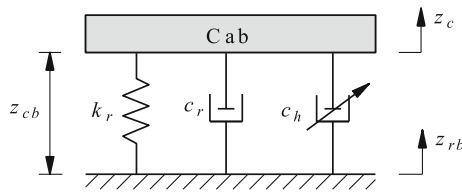


Fig. 2 Lumped parameter model of the cab's hydraulic mount

in $F(t)$ are calculated in Sect. 2.2 while the excitation force F_s of the driver's seat suspension in $F(t)$ is calculated in Sect. 3.

2.2 Force excitations of the vibratory roller

2.2.1 Force excitation of the cab isolations

The cab isolations of the vibratory roller were used by four rubber mounts to isolate the vibrations of the cab. The existing studies indicated that the cab's rubber mounts replaced by using the hydraulic mounts better ameliorated the ride comfort of the vibratory roller [1, 2]. Thereby, in this study, the hydraulic mounts of the cab isolation are used to ameliorate the vibratory roller's ride comfort. The dynamic model of the cab's hydraulic mount is plotted in Fig. 2. Where c_r, k_r, c_h are the damping coefficient of the rubber mount, stiffness coefficient of the rubber mount, and fluid's damping coefficient in the hydraulic mount.

Based on the study result in Refs. [3, 4], the excitation force F_{ci} of the cab's hydraulic mount was calculated by:

$$F_{ci} = (c_{ci}\dot{z}_{cbi} + k_{ci}z_{cbi}) + c_{hi}|\dot{z}_{cbi}|\dot{z}_{cbi}$$

$$z_{cbi} = z_c - z_{rb} + (-1)^{u+1}\varphi_c l_{u+1} - \varphi_{rb}l + \dots$$

$$+ (-1)^{i+1}(\theta_c - \theta_{rb})b_v \tag{2}$$

where $\begin{cases} i = 1 - 2 \\ i = 3 - 4 \end{cases}$ then $\begin{cases} u = 1, l = l_1 + l_2 + l_3 \\ \text{, and } v = i + 1 \\ u = 2, l = l_4, \text{ and } v = i - 1 \end{cases}$.

2.2.2 Force excitation of the wheels

When the vibratory roller is moving and working on the deformable terrain with the random terrain surface, under the influence of the static and dynamic loads of the wheel, two different deformations of the wheel and terrain contact are appeared including (1) only the terrain's deformation (region of ba) and (2) the deformation of both wheel and terrain (region of $b'ob$), as shown in Fig. 3. Where r_w is the radius and m_w is the mass of the wheel; z_w is the dynamic displacement of the wheel; z_{w0} is the static deformation of the wheel; and z_x is the sinkage of the deformable terrain.

The pressure p and the shear stress τ arising from the soil compression in the deformable regions of ba and $b'ob$

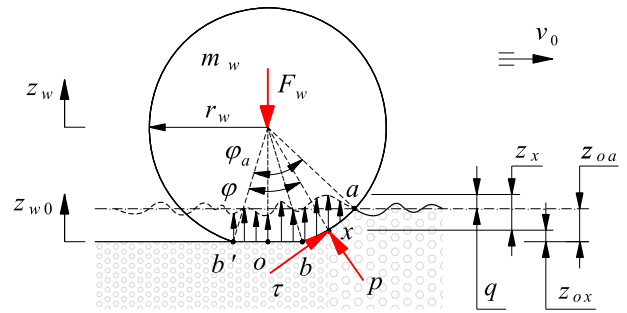


Fig. 3 The wheel-deformable terrain contact model

thus impact the wheel. Thus, the reaction force F_{gw} of the deformable terrain under the wheel is given as follows [15, 16]:

$$F_{gw} = \int_0^{\varphi_a} B_w r_w p \cos \varphi d\varphi + \int_0^{\varphi_a} B_w r_w \tau \sin \varphi d\varphi \tag{3}$$

Both p and τ are given by Bakker as follows [16]:

$$p = (k_\theta + k/B_w)z_x^n \text{ and } \tau = (p \tan \theta + c)(1 - e^{-j/K}) \tag{4}$$

where k and k_φ are the soil stiffness coefficients for sinkage and internal friction; n is the sinkage exponent; B_w is the width of the wheel; c is the soil cohesion coefficient; and $z_x = z_{oa} + q - z_{ox} = q + z_w - z_{w0} - z_{ox}$, herein, q is the terrain surface excitation and it is described as follows.

According to ISO/TC108/SC2/WG4 [17], the power spectral density (PSD) of the terrain surface roughness $S(\psi)$ is written as [17, 18]:

$$S(\psi) = S(\psi_0) \left(\frac{\psi}{\psi_0} \right)^{-w_0}, \quad w_0 = \begin{cases} 3 & \psi \leq \psi_0 \\ 2.25 & \psi > \psi_0 \end{cases} \tag{5}$$

The value $S(\psi_0)$ provides a measure for the random terrain with the reference spatial frequency $\psi_0 = 1/2\pi$ (cycle/m). Based on the white noise signal of the random function (w) and $S(\psi)$ of the terrain surface at a constant speed v_0 of the vibratory roller, the terrain irregularities q can then be simulated by [7]:

$$\dot{q} + 2\pi n_0 v_0^2 q = 2\pi n_0 \sqrt{S(n_0) v_0 w} \tag{6}$$

Four different levels of the good-, medium-, poor-, and very poor-surface of the terrain surface established based on their PSD value were proposed to calculate the q [19]. Thus, the desired terrain roughness can be yielded by choosing a value in four different levels of the terrain surface roughness.

According to the dynamic model of the vibratory roller in Fig. 1 and the wheel-deformable soil contact model in Fig. 3,

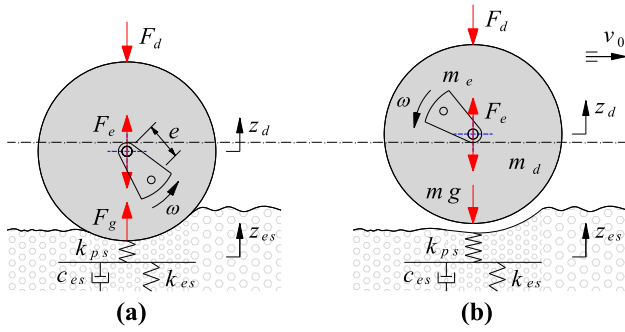


Fig. 4 The drum-elastoplastic soil interaction model: **a** loading phase; **b** drum-hop phase

the force responses F_{wj} of wheels are described as:

$$F_{wj} = c_{wj}\dot{z}_j + k_{wj}z_j$$

$$F_{gwj} + F_{wj} = m_{wj}g \tag{7}$$

where $z_j = z_{rb} - \varphi_{rb}l_5 - z_{wj} + (-1)^j\theta_{rb}b_{j+3}, j = 1-2$.

2.2.3 Force excitation of the vibratory drum

The vibratory rollers use the most of its time to work on the elastoplastic soil ground. Thereby, according to Adam and Kop [1], a model of the rigid drum and elastoplastic soil interaction is built in Fig. 4 to determine the force excitation F_d of the vibratory drum. The elastoplastic property of soil can be expressed via a plasticity factor ε and a damping ratio of plastic soil γ as:

$$\varepsilon = \frac{k_{ps}}{k_{ps} + k_{se}} \text{ and } \gamma = \frac{c_{se}}{k_{ps}} \tag{8}$$

where ε is the compression ratio; k_{se} is the elastic stiffness; k_{ps} is the compression stiffness; c_{se} is the compression damper, respectively.

In a vibration cycle of the rigid drum-elastoplastic soil interaction, there are two or three distinct phases that occur in the motion of the drum and they are described as follows:

Loading phase: The gravel-soil ground is compressed by the drum. The density is thus increased and it has become elastic. The elastic stiffness and compression stiffness of the gravel-soil ground are increased while the compression damper is decreased. In order to describe the relation of z_d, ε , and γ , the vibration equation of the rigid drum is expressed as [1]:

$$\varepsilon\gamma m_d \ddot{z}_d + m_d \ddot{z}_d = \varepsilon\gamma \dot{F}_d + F_d - \varepsilon c_{es} \dot{z}_d + \dots$$

$$+ (\varepsilon - 1)k_{ps}z_d + \varepsilon\gamma m_e e \omega^3 \cos \omega t$$

$$+ m_e e \omega^2 \sin \omega t \tag{9}$$

where $\omega = 2\pi f$ is the frequency excitation of the drum.

Unloading phase: The rigid drum moves upward, and the gravel-soil ground is restored. The vibration equation of the rigid drum is expressed by:

$$m_d \ddot{z}_d = F_d - c_{es} \dot{z}_d + m_e e \omega^2 \sin \omega t \tag{10}$$

Drum-hop phase: The gravel-soil ground has become elastic, and the drum is easy to separate from the soil ground surface. The vibration equation of the rigid drum is expressed by:

$$m_d \ddot{z}_d = F_d + m_g + m_e e \omega^2 \sin \omega t \tag{11}$$

Based on the rigid drum-elastoplastic soil interaction model in Fig. 4 and the model of the drum’s isolation in Fig. 1, the motion equations of the drum and force excitation of the drum isolation are described as [1, 2]:

$$m_d \ddot{z}_d = F_d - F_g + m_e e \omega^2 \sin \omega t$$

$$F_d = c_{dj}(\dot{z}_{fbj} - \dot{z}_{dj}) + k_{dj}(z_{fbj} - z_{dj})$$

$$F_g = c_{es} \dot{z}_{es} + k_{es} z_{es} = k_{ps}[z_d - (q - z_{es})] \tag{12}$$

where $z_{fbj} - z_{dj} = z_{fb} - z_d + (-1)^j(\theta_{fb} - \theta_d)b_{3+j}, j = 1-2$.

By combining Eqs. (9–12), the force excitation F_d of the vibratory drum is then determined.

3 Seat’s semi-active suspension

3.1 Seat’s suspension equipped with QZSS

3.1.1 The term and characteristics of QZSS

In a typical structure using the elastic spring, an increase in force F causes an increase in deformation z and vice versa ($F = kz$). Thus, the dynamic stiffness k is defined as the "positive stiffness" of the elastic spring, as shown in Fig. 5 with "positive stiffness". On the contrary, with a structure using the symmetrical elastic bars or symmetrical springs, during some regions of the force and deformation relationship, there exhibit reducing force F with increasing deformation z , thus, the dynamic stiffness k is defined as the "negative stiffness" of the structure, as plotted in Fig. 5 with "negative stiffness".

With a structure combined with both "positive stiffness" and "negative stiffness", during some regions of the force and deformation relationship, there exhibit a constant force F with increasing deformation z , thus, the dynamic stiffness k is defined as the "quasi-zero-stiffness" of the structure, as depicted in Fig. 5 with "quasi-zero-stiffness". Based on the force–deformation characteristic of the quasi-zero-stiffness structure (QZSS), the QZSS is then researched and added to the seat’s semi-active suspension to improve the vibratory roller’s ride comfort.

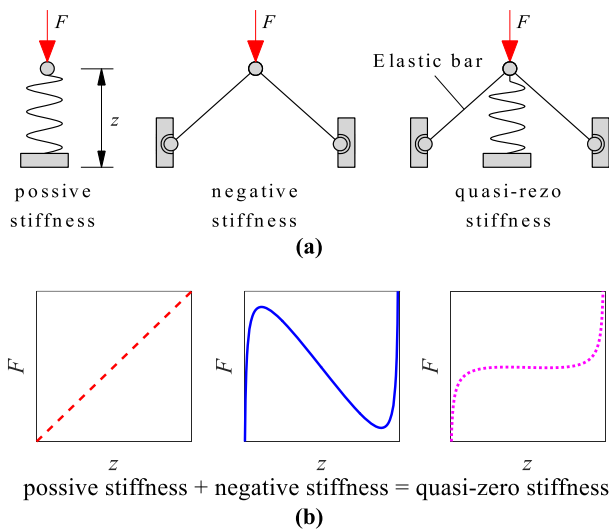


Fig. 5 QZSS's model and characteristic: **a** QZSS's model; **b** characteristic of the restoring force–deformation

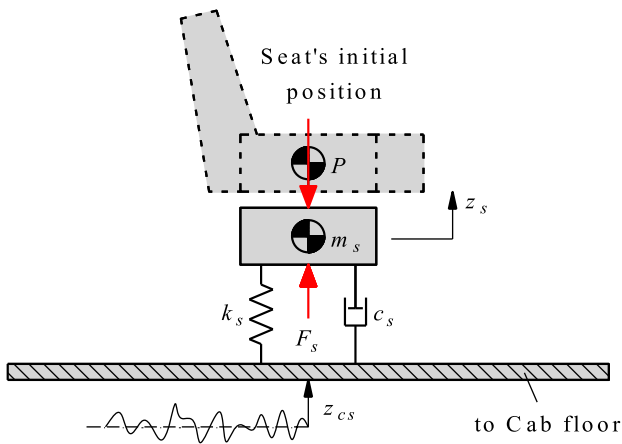


Fig. 6 Modeling of the seat's passive suspension

3.1.2 Modeling of seat's semi-active suspension equipped with QZSS

In the seat's passive suspension used on the vibratory roller, this passive suspension had been designed by a passive damper and a passive spring characterized by a passive damping coefficient c_s and passive stiffness coefficient k_s [2, 3], as shown in Fig. 6.

Based on the model of the vibratory roller dynamic in Fig. 1 and the model of the seat's passive suspension in Fig. 6, the vertical force response of the seat's passive suspension (F_s) is written as follows:

$$F_s = c_s \dot{z} + k_s z \tag{13}$$

where $z = z_s - z_{cs} = z_s - z_c + \phi_c l_1 + \theta_c b_1$.

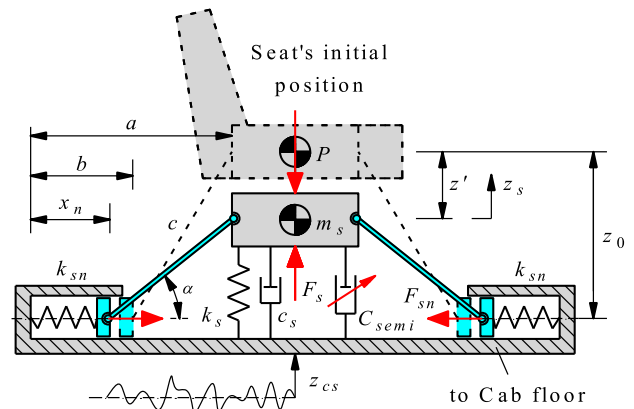


Fig. 7 Modeling of the seat's semi-active suspension equipped with QZSS

To improve the ride comfort of the vibratory roller, the cab's isolation systems were mainly optimized or controlled, while the seat's isolation was always equipped with passive suspension [3, 4]. Thus, it is difficult to ensure the vehicle's ride comfort according to the standard of ISO 2631-1 [5]. In order to ameliorate the ride comfort of the vibratory roller, the seat's passive suspension had been added by a semi-active damping coefficient (C_{semi}) and QZSS. Its dynamic model is shown in Fig. 7. Where k_n is the stiffness coefficient of two steel springs of the QZSS installed horizontally and symmetrically on the cab floor; a is the distance between the wall and seat; b is the initial length of the horizontal spring; c is the length of the hard guide bar used to link between the driver's seat and horizontal spring; x is the length after deformation of the horizontal spring; and z_0 is the distance between the seat's initial position and cab's floor.

To reduce the computational complexity of the seat's semi-active suspension equipped with the QZSS, some assumptions are given to overcome some limitations of the model as follows: (1) the vibration of the semi-active seat suspension embedded by QZSS is mainly calculated in the vertical direction; (2) the friction force between the hard bar and horizontal spring is very small and it is also ignored; (3) the mass of the hard bar is very small and it is also ignored, and (4) the semi-active damper in the seat's semi-active suspension is modeled by a semi-active damping coefficient C_{semi} controlled by the fuzzy controller.

Under the impaction of the static load of the driver's seat ($P = m_s \times g$), the seat's suspension is then deformed downward by z' . Therefore, the vertical force response of the seat's suspension F_s is calculated as follows:

$$F_s = (c_s \dot{z} + k_s z) + C_{semi} \dot{z} + F_{QZSS} \tag{14}$$

$$F_{QZSS} = 2F_{sn} \tan \alpha = 2k_n(b - x)(z_0 - z') / (a - x) \tag{15}$$

where F_{QZSS} is the restoring force of the QZSS.

Based on the correlation between the initial position and the equilibrium position of the driver’s seat in Fig. 7, the values of z_0 and x in Eq. (15) are determined by:

$$z_0^2 = c^2 - (a - b)^2 \text{ and } x = a - \sqrt{c^2 - (z_0 - z')^2} \quad (16)$$

By substituting Eq. (16) into (15), the restoring force of the QZSS in Eq. (15) has been rewritten as follows:

$$F_{QZSS} = \alpha k_s \left(1 + \frac{1 - \beta_2}{\sqrt{\beta_1^2 - (z_0 - z')^2/b^2}} \right) (z_0 - z') \quad (17)$$

where $\alpha = 2k_n/k_s$ is the stiffness ratios, $\beta_1 = c/b$ and $\beta_2 = a/b$ are the ratios of the QZSS’s geometrical dimension.

Under the vibration excitation of the cab’s floor (z_{cs}) at the seat’s suspension position, the vibration response of the driver’s seat is then created by z_s , as shown in Figs. 6 and 7. Thereby, the motion equation of the driver’s seat in four cases including (1) the seat’s passive suspension (PS), (2) the seat’s semi-active suspension (SAS), (3) the seat’s passive suspension added by QZSS (PS + QZSS), and (4) the seat’s semi-active suspension added by QZSS (SAS + QZSS) is written by:

$$m_s \ddot{z}_s = -[(c_s \dot{z} + k_s z) + C_{semi} \dot{z} + \alpha k_s (1 + \Pi)(z_0 - z')] \quad (18)$$

$$\begin{cases} C_{semi} = 0 \text{ and } \alpha = 0 \text{ with PS} \\ C_{semi} > 0 \text{ and } \alpha = 0 \text{ with SAS} \\ C_{semi} = 0 \text{ and } \alpha > 0 \text{ with PS + QZSS} \\ C_{semi} > 0 \text{ and } \alpha > 0 \text{ with SAS + QZSS} \end{cases}$$

where $\Pi = (1 - \beta_2)/\sqrt{\beta_1^2 - (z_0 - z')^2/b^2}$; $z = z_0 - z'$;

Equation (18) is then applied for the simulation to assess the ride comfort of the vibratory roller as well as the isolation performance of the seat’s semi-active suspension embedded by QZSS.

3.2 Application of fuzzy controller for seat’s SAS

To control the semi-active suspension system of the vehicles, the control methods of Neuro control, PID control (P, PI, PID), Fuzzy control, or Feedback control were applied for controlling the damping coefficient of the semi-active suspensions of the vehicle and cab [3, 4, 8–10]. With the classic linear controller of the P, PI, or PID controller, it is one of the controllers with not only a simple structure but also robust performance, and it is generally used in industrial process control. However, its control performance depends on the appropriate selection of the coefficients of the proportional

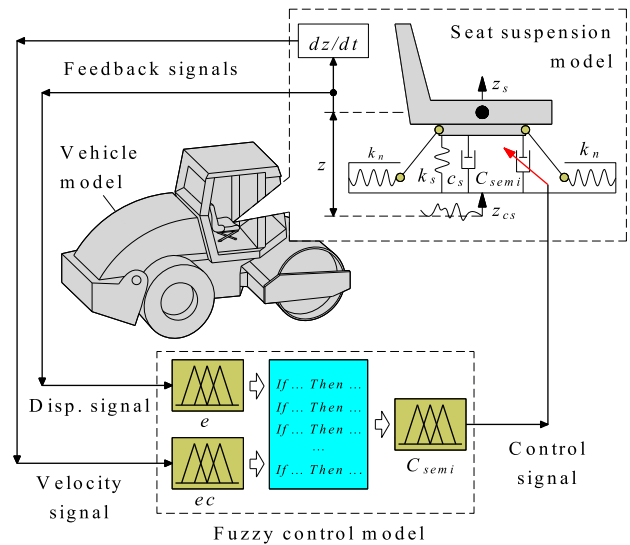


Fig. 8 The model of the seat’s semi-active suspension controlled by the fuzzy controller

k_p , integral k_i , and derivative k_d . The Ziegler-Nichols technique was applied to choose the coefficients of k_p , k_i , and k_d . But it was only efficient when the system worked at the designed operating condition [3, 10]. On the contrary, the fuzzy controller created by Zadeh in 1965 was widely used in different fields. It could control the suspension systems under all the various operating conditions and its control performance was good and stable. But its performance greatly depended on the fuzzy control rules [3, 7]. To enhance the control performance of the fuzzy controller, the genetic algorithm was applied to optimize the control rules. The fuzzy controller with its optimal control rules was then applied to control the semi-active suspension system of the vehicles [3, 6–8]. With the seat’s semi-active suspension of the vibratory roller, the fuzzy controller with its optimal control rules is applied for controlling the C_{semi} .

To control the C_{semi} of the seat’s semi-active suspension using the fuzzy controller, two feedback signals of the vertical displacement " $e = z = z_s - z_{cs}$ " and velocity " $ec = dz/dt$ " generated by the driver seat’s suspension when the vibratory roller is working are used as two input variables of the fuzzy controller. Based on these two input signals, the fuzzy controller will calculate and give one output control variable of the C_{semi} through the control rules of the fuzzy controller. The control model of the vibratory roller’s seat suspension using the fuzzy controller is plotted in Fig. 8.

The fuzzy controller includes the Fuzzification interface, Fuzzy inference system, and Defuzzification interface. First, the crisp values in Fuzzification are transformed into the linguistic variables, then, the Fuzzy inference system is used by control rules in accordance with inference rules, finally, the LV is transformed back to crisp values via Defuzzification

for use by the physical plant [20]. The design of the fuzzy controller is performed via three steps as follows:

Step 1 of defining and setting the linguistic variables of input/output values: The linguistic variables of both the displacement and velocity of the seat's suspension (e and ec) are defined by Negative-Big (NB), Negative-Small (NS), Zero (Z), Positive-Small (PS), and Positive-Big (PB). Concurrently, the linguistic variable of C_{semi} is defined by Small (S), Medium-Small (MS), Medium (M), Medium-Big (MB), and Big (B), respectively. The numerical values with their linguistic variables are established in Table 1. The boundary conditions of the e , ec , and C_{semi} are established by $-0.02 \leq e \leq +0.02$ (m), $-0.30 \leq ec \leq +0.03$ (m/s), and $0.1 \leq C_{semi} \leq 1.5$ (kNs/m).

Step 2 of setting the membership function of the fuzzy controller: The membership function of the input/output variables is established by using the Triangular function in the fuzzy controller, as shown in the same Fig. 8 with "Fuzzy control model".

Step 3 of setting the control rules: Based on the control rules of the fuzzy controller optimized in Ref. [8], as listed in Table 2, these optimal control rules are then used to control the semi-active damping coefficient C_{semi} . The control rules between the e , ec , and C_{semi} have been established as follows:

- (1) If ec is NB and e is NB then C_{semi} is B,
- (2) If ec is NS and e is NB then C_{semi} is MB,
- ...
- (25) If ec is PB and e is PB then C_{semi} is B.

Based on the numerical values of the of e and ec ; and optimal control rules, the minimum function and centroid method in the tools of the fuzzy controller are then selected to compute the value of C_{semi} .

4 Results and discussion

4.1 Evaluation criteria

The efficiency of the vehicle's suspension system had been mainly assessed through the ride comfort, the deformation of the suspension system, and road friendliness [3, 4, 7]. With the index of the ride comfort of the vehicle or the driver, it was assessed via the weighted root-mean-square acceleration of the driver's seat (a_{ws}) [4, 5, 12]. Additionally, according to the standard of ISO 2631-1 [5], the index of the power spectral density (PSD) acceleration was also used to assess the influence of the vibration on the health and endurance limit of the human body. The value of a_{ws} of the driver's seat

had been expressed as follows [5, 7]:

$$a_{ws} = \sqrt{\frac{1}{T} \int_0^T \ddot{z}_s^2(t) dt} \tag{19}$$

where $\ddot{z}_s(t)$ is the seat's acceleration response in the simulation time region of T (s).

In order to assess the ride comfort of the vibratory roller as well as the isolation performance of the seat's semi-active suspension embedded by QZSS, two indexes of the a_{ws} and maximum PSD acceleration of the driver's seat are chosen as the objective functions.

4.2 Isolation performance of the seat's SAS equipped with the QZSS

The vibratory roller mainly works on the elastoplastic soil ground. Therefore, to assess the seat's semi-active suspension embedded by the QZSS on ameliorating the ride comfort of the driver's seat, the dynamic parameters of the vibratory roller listed in Table 3 [4], the optimized parameters of the QZSS listed in Table 4 [12], the parameters of a poor terrain surface listed in Table 5 [19], and the parameters of the elastoplastic terrain under the wheels and drum listed in Table 6 [1–3] are used to simulate the vibration of the vibratory roller when the vehicle is moving and working at $v_0 = 1.67$ m/s under an excitation $f = 28$ Hz of the vibratory drum.

The simulation results of the acceleration response and weighted root-mean-square acceleration (a_{ws}) of the driver's seat with four different cases of (1) PS, (2) SAS, (3) PS + QZSS, and (4) SAS + QZSS are shown in Fig. 9a–b.

The acceleration response in Fig. 9a shows that the driver's seat acceleration with the SAS is smaller than that of the PS. This is due to the semi-active damping coefficient of C_{semi} in Eq. (14) controlled by the fuzzy controller to reduce the vibration of the driver's seat. With the PS + QZSS, the acceleration response of the driver's seat is obviously reduced compared to both PS and SAS. This is due to the influence of the restoring force F_{QZSS} of the QZSS in Eq. (17). In the existing research, with the QZSS added into the seat's passive suspension, the ride comfort of the driver's seat is better than the seat's passive suspension without QZSS [11–14]. Besides, this study also shows that with the PS + QZSS, the acceleration response of the driver's seat is significantly decreased compared to the SAS. This implies that the QZSS ameliorates the driver's seat ride comfort better than the SAS. With the SAS + QZSS, the acceleration response of the driver's seat is significantly reduced in comparison with the PS + QZSS. This result is also due to the influence of both the semi-active damping coefficient of C_{semi} and restoring force F_{QZSS} of the QZSS in Eqs. (14) and (17).

Table 1 The language variables (LV) and their numerical values

Input variables			Output variables	
LV	e (m)	ec (m/s)	LV	$C_{semi} \times 10^3$ (Ns/m)
NB	- 0.02	- 0.30	S	0.1
NS	- 0.01	- 0.15	MS	0.4
Z	0	0	M	0.8
PS	0.01	0.15	MB	1.2
PB	0.02	0.30	B	1.5

Table 2 Optimal control rules of the fuzzy controller

C_{semi}		e				
		NB	NS	Z	PS	PB
ec	NB	B	B	MB	S	S
	NS	MB	M	MS	S	MS
	Z	MB	MS	S	MS	M
	PS	MS	S	MS	M	B
	PB	S	MS	MS	M	B

Table 3 Vibratory roller’s dynamic parameters

Parameters	Values	Parameters	Values
m_s (kg)	85	c_{d1-2} (Ns/m)	2.9×10^3
m_c (kg)	891	$c_{w1,2}$ (Ns/m)	4.0×10^3
m_{fb} (kg)	2822	b_1 (m)	0.55
m_{rb} (kg)	4464	b_2 (m)	0.7
m_d (kg)	4378	b_3 (m)	0.68
k_s (N/m)	5.8×10^3	b_4 (m)	0.945
k_{c1-2} (N/m)	0.91×10^6	b_5 (m)	0.945
k_{c3-4} (N/m)	0.12×10^6	l_1 (m)	0.383
k_{d1-2} (N/m)	3.90×10^6	l_2 (m)	0.1
k_{w1-2} (N/m)	0.50×10^6	l_3 (m)	0.524
c_s (Ns/m)	120	l_4 (m)	0.136
c_{c1-2} (Ns/m)	0.218×10^3	l_5 (m)	0.6
c_{c3-4} (Ns/m)	0.029×10^3	l_6 (m)	0.76
c_{h1-2} (Ns ² /m ²)	20×10^3	l_7 (m)	0.9
c_{h3-4} (Ns ² /m ²)	4.5×10^3	l_8 (m)	1.5

Table 4 The design parameters of the QZSS

Parameters	a (m)	β_1	β_2	α
Values	0.286	0.73	1.17	0.63

Table 5 The numerical values of poor terrain surface

Parameters	$S(\psi_0)$ (m ³ /cyc)	w_0
Values	3782.5×10^{-6}	2.14

Table 6 The numerical values of elastoplastic soil ground

Parameters	Values	Parameters	Values
<i>Deformable soil ground under the wheels</i>			
θ ($^\circ$)	29.8	k_θ (MN/m $^{n+2}$)	5.88
k (N/m $^{n+1}$)	6	c (Pa)	310
<i>Elastoplastic soil ground under the drum</i>			
ε	0.87	k_{es} (MN/m)	42.3
k_{ps} (MN/m)	283	c_{es} (kNs/m)	37.1

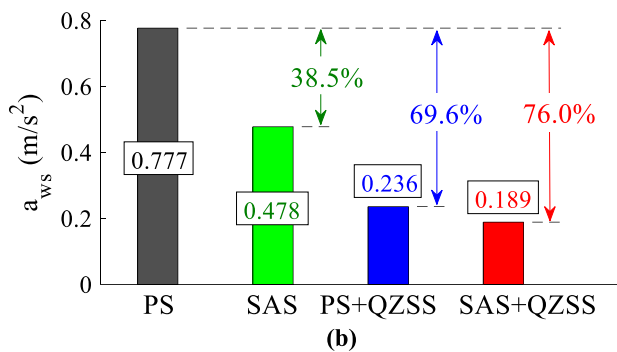
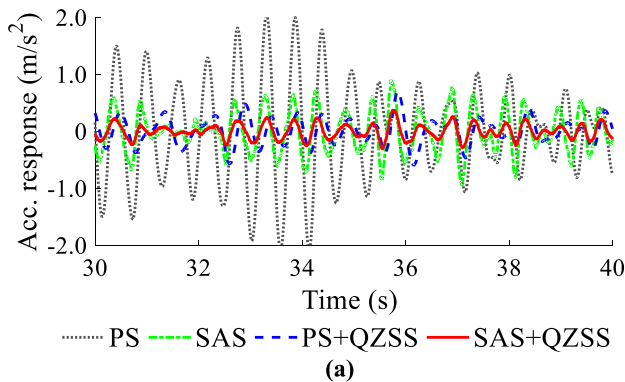


Fig. 9 The acceleration of the driver's seat: **a** acceleration response; **b** weighted root-mean-square acceleration

In addition, based on the driver's seat acceleration response in Fig. 9a, the a_{ws} is also computed and plotted in Fig. 9b. The result indicates that the a_{ws} with SAS, PS + QZSS, and SAS + QZSS is greatly decreased by 38.5%, 69.6%, and 76.0% in comparison with PS, respectively, especially with SAS + QZSS. Therefore, the driver's seat ride comfort with SAS + QZSS is improved better than that of SAS and PS + QZSS.

Besides, the acceleration response of the driver's seat in the frequency region is also presented to evaluate the isolation performance between the SAS, PS + QZSS, and SAS + QZSS. The results of the PSD acceleration response of the driver's seat are plotted in Fig. 10. The results indicate that the PSD acceleration response of the driver's seat with SAS,

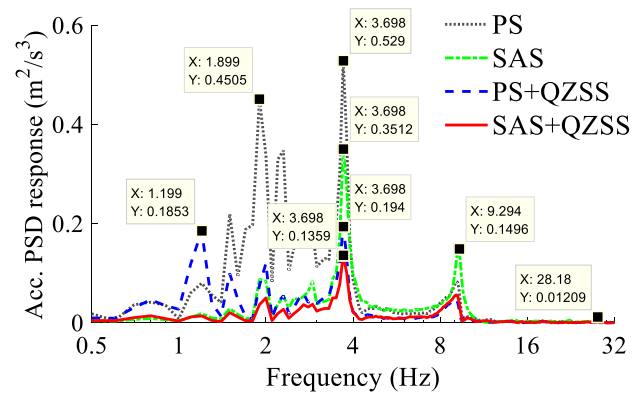


Fig. 10 Seat's PSD acceleration responses

Table 7 Maximum PSD value of the driver's seat acceleration

Isolations	Frequency (Hz)	Maximum PSD (m^2/s^3)
PS	3.698	0.529
SAS	3.698	0.351
PS + QZSS	3.698	0.194
SAS + QZSS	3.698	0.136

PS + QZSS, and SAS + QZSS is also greatly reduced in comparison with PS, especially with the seat's suspension using SAS + QZSS. This is also due to the influence of both values of C_{semi} and F_{QZSS} in Eqs. (14) and (17). Especially, at a low-frequency region from 0.5 to 4.0 Hz which greatly affects the driver's health and safety [7], the maximum PSD value of the driver's seat acceleration listed in Table 7 shows that the maximum PSD acceleration of the driver's seat with SAS, PS + QZSS, and SAS + QZSS is greatly reduced by 33.6%, 63.3%, and 73.4% compared to the seat's passive suspension, respectively, especially with SAS + QZSS. Therefore, with the QZSS added into the seat's semi-active suspension, the ride comfort of the driver's seat is greatly improved in both time and frequency regions. However, in this part, the isolation performance of SAS + QZSS only assesses under one vibratory roller's working condition. To fully assess the isolation performance as well as the stability of SAS + QZSS,

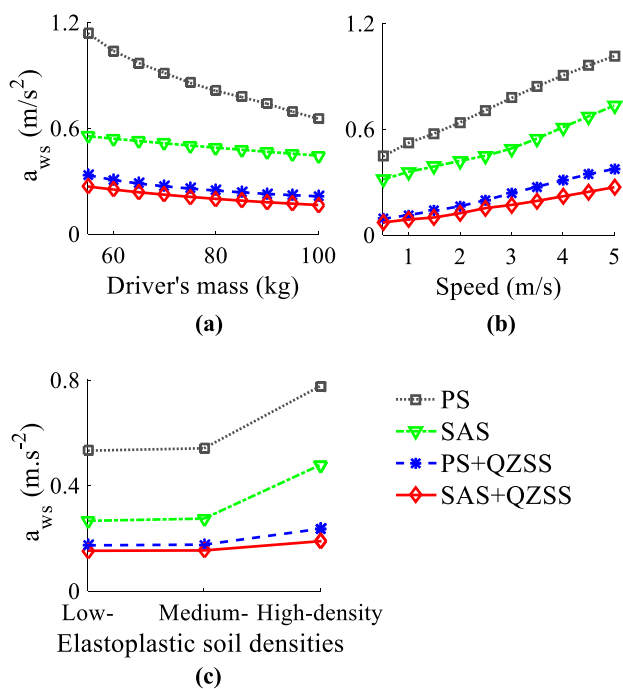


Fig. 11 The result of a_{ws} under various operating conditions of the vehicle: **a** change of driver's mass; **b** change of vehicle's velocity; **c** change of elastoplastic soil grounds

the various operating conditions of the vibratory roller such as the vehicle's moving velocity, driver's mass, and elastoplastic soil ground should be also simulated and evaluated.

4.3 Isolation performance under the different operating conditions of the vehicle

Under the same simulation condition in Sect. 4.2, the change of the driver's mass, vehicle's speed, and elastoplastic soil ground is simulated for assessing the isolation performance and stability of the SAS + QZSS.

Under the change of the driver's mass: A driver's mass range of $m_s = [55, 60, \dots, 100]$ (kg) is simulated. The calculation result of the a_{ws} is shown in Fig. 11a. Figure 11a shows that the value of a_{ws} with the seat's suspension using the PS, SAS, PS + QZSS, and SAS + QZSS is reduced with the increase of the driver's mass and vice versa. Thus, the driver's ride comfort is remarkably affected by the change of the driver's mass. However, the value of a_{ws} with SAS + QZSS is not only decreased in comparison with PS, SAS, and PS + QZSS but also stable under various values of the driver's mass.

Under the change of the vehicle's moving velocity: A velocity range of $v_0 = [0.5, 1.0, \dots, 5.0]$ (m/s) is also simulated. The result of the a_{ws} is calculated and plotted in Fig. 11b. The result shows that the value of a_{ws} with all PS, SAS, PS + QZSS, and SAS + QZSS is also increased

Table 8 Parameters of three elastoplastic soil grounds

Elastoplastic soils	Low-	Medium-	High-density
ε	0.34	0.72	0.87
k_{sp} (MN/m)	6.44	82.1	283
k_{se} (MN/m)	12.5	31.9	42.3
c_{se} (kNs/m)	70.0	43.4	37.1

with the increase of the vibratory roller's moving velocity and vice versa. This means that the driver's ride comfort is significantly reduced when the vehicle's moving velocity is increased. With the SAS + QZSS used in the seat's suspension, the value of a_{ws} is lower than that of PS, SAS, and PS + QZSS under various moving velocities of the vibratory roller. Thus, the seat's semi-active suspension added by QZSS can improve the vibratory roller's ride comfort under all the vehicle's moving velocities.

Under the change of the elastoplastic soil grounds: In the working condition of the vibratory drum on the elastoplastic soil ground, the density of the elastoplastic soil ground was changed and remarkably influenced the ride comfort of the driver [1–3, 21]. The research result in Ref. [1] showed that in the interaction process between the drum and elastoplastic soil ground, the elastoplastic soil characteristic was varied via three different stages including (1) the initial stage, the drum compacted on the elastoplastic soil ground with the soil property being relatively soft (low-density), (2) the density ε of the soil ground was then increased in the repeated compression of the drum and soil ground interaction (medium-density), and (3) the final stage, the soil ground's density continued to be increased until the contact between the drum and soil ground was broken (high-density). Based on the parameters of three elastoplastic soil grounds with the low-, medium-, and high-soil densities listed in Table 8 [1, 21], the influence of the elastoplastic soil grounds on the ride comfort of the vibratory roller and the performance of the driver's seat suspension system is then simulated. The calculation result of a_{ws} is depicted in Fig. 11c.

The result shows that the value of a_{ws} with PS, SAS, PS + QZSS, and SAS + QZSS is remarkably affected by the different soil densities of the elastoplastic soil ground. Under a soil ground with the low-density, the a_{ws} is small. This means that the driver's ride comfort is improved on elastoplastic soil ground with the low-density. When the soil ground's density is increased up to the medium-density after the repeated compression of the vibratory drum on the elastoplastic soil ground, the damping characteristic (c_{se}) of the soil ground is decreased while the elastoplastic stiffness characteristics (k_{sp} and k_{se}) of the soil ground is increased, thus, the soil ground becomes harder and more elastic. As a result, the a_{ws} are slightly increased. When the density of the soil ground

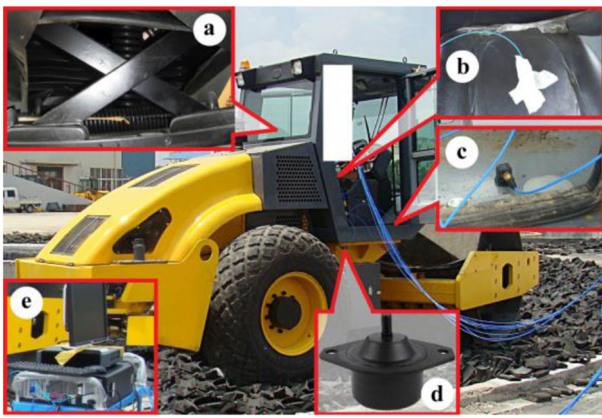


Fig. 12 The vibratory roller's experimental model with the cab isolation using the hydraulic mounts and the seat's passive suspension embedded by QZSS: **a** QZSS; **b** seat's acceleration sensor; **c** acceleration sensor on the cab's floor; **d** hydraulic mount; **e** displace of the experimental result

is continuously increased up to the high-density, the a_{ws} is strongly increased. This means that the ride comfort of the driver is strongly reduced under an elastoplastic soil ground with the high-density. This result is also similar in Refs. [2, 3].

By using the SAS + QZSS, the a_{ws} is also smaller than that of PS, SAS, and PS + QZSS under the elastoplastic soil ground with different densities. Thus, with the QZSS embedded in the seat's semi-active suspension, the ride comfort of the driver is improved under the different working conditions of the vibratory roller.

4.4 Experimental investigation

In order to verify the study result of the 3-D vehicle dynamic model, a vibratory roller with the cab isolation equipped with the hydraulic mounts and seat's passive suspension added by the QZSS is used for the experiment. The experiment of the vibratory roller is performed under the same simulation condition of the vehicle in Sect. 4.2. The vehicle's experiment model is shown in Fig. 12.

In order to determine the acceleration response and PSD acceleration of the driver's seat, an acceleration sensor is installed on the driver's seat to measure the seat's acceleration response. The dynamic test and analysis system of the Belgium LMS are then used to calculate and display the measured results. The acceleration response and the PSD acceleration of the driver's seat are plotted in Fig. 13a–b.

The result in Fig. 13a indicates that the acceleration response of the driver's seat in the simulation is similar to like the experiment. Moreover, the value of a_{ws} in the simulation is only higher than that of the experiment by 8.47%. Besides, the PSD value of the driver's seat acceleration in Fig. 13b shows that the resonance peaks of the seat's PSD

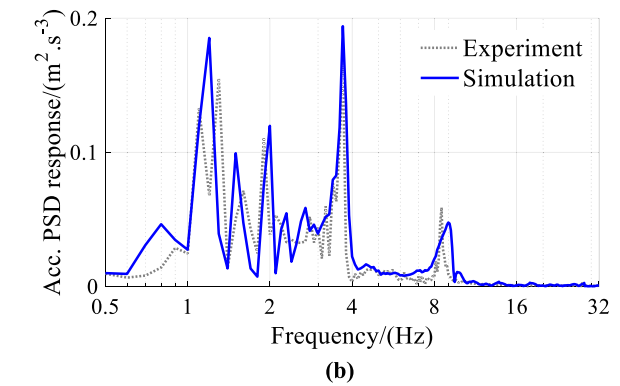
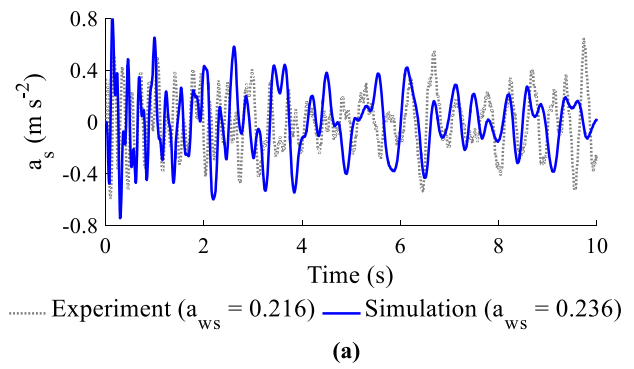


Fig. 13 The experimental results of the driver's seat vibration: **a** acceleration response; **b** PSD acceleration response

acceleration of the simulation are also similar to like the experiment in all the responses and trends. However, the results in Figs. 13a–b also show that the comparative results between the experiment and simulation of the seat's acceleration response and the seat's PSD acceleration have a small error. This can be due to the influence of some deviations of the dynamic parameters of the QZSS, vibratory roller, and elastoplastic soil ground in the simulation; or the influence of the small error during the installation of the experimental equipment. However, these deviations insignificantly influence the study result and they can be accepted. Thus, based on the experiment and simulation of the seat's semi-active suspension added by the QZSS, the SAS + QZSS should be used on the seat's suspension of the vibratory roller to further improve the ride comfort of the driver.

5 Conclusions

With the semi-active damping coefficient of C_{semi} is controlled by the fuzzy controller, the driver's seat ride comfort is significantly improved in comparison with the seat's passive suspension; while with the seat's passive suspension added by the QZSS, the driver's seat ride comfort is improved better than the seat's semi-active suspension.

With the seat's semi-active suspension added by the QZSS, the value of a_{ws} and maximum PSD value of the seat's acceleration are remarkably reduced in comparison with PS, SAS, and PS + QZSS. Especially, the a_{ws} and maximum PSD value of the driver's seat acceleration with SAS + QZSS are greatly decreased by 76.0% and 73.4% in comparison with the seat's passive suspension.

Based on the experiment and numerical simulation of the vibratory roller with the driver's seat suspension equipped with PS, SAS, PS + QZSS, and SAS + QZSS, the seat's semi-active suspension added by the QZSS should be applied to further enhance the vibratory roller's ride comfort. Moreover, this research not only contributes to the existing body of knowledge on off-road vibratory rollers but also could provide an important reference for the application of the QZSS on the driver's seat semi-active suspension of other vehicles to further ameliorate the vehicle's ride quality.

Author contributions All authors contributed to the study conception and design. Material preparation, data collection, models of the vibratory roller, semi-active seat suspension, and QZSS as well as calculation of the dynamic equations were performed by Tianfeng Ye. The first draft of the manuscript was written by Vanliem Nguyen. The simulation and analysis the results were performed by Shiming Li. All authors read and approved the final manuscript.

Funding This work has been supported by the Guidance Project of Science and Technology Research Program of Education Department of Hubei Province, China (No. B2022254).

Data availability All data generated or analyzed during this study are included in this published article.

Code Availability The MATLAB code used for the simulation can be provided via email if required.

Declarations

Conflict of interest Tianfeng Ye is a lecturer at School of Electrical and Electronic Information Engineering, Hubei Polytechnic University, Huangshi, China. Her current research interests include control system, optimal design, and stability of vibration system. Vanliem Nguyen is a doctor at School of Mechanical and Electrical Engineering, Hubei Polytechnic University, Huangshi, China. His current research interests include vehicle dynamics, vibration and optimization control, and lubrication in the engine. Shiming Li is a lecturer at School a doctor at School of Mechanical and Electrical Engineering, Hubei Polytechnic University, Huangshi, China. His current research interests include vehicle dynamics, vibration and optimization control.

References

- Adam D, Kopf F (2000) Theoretical analysis of dynamically loaded soils. European workshop compaction of soils and granular materials. Paris, France 2000: 207–220
- Le V (2013) Vibration study and control for cab of vibratory roller. Southeast University, Nanjing
- Zhang J, Yang Z et al (2019) Low-frequency performance of semi-active cab's hydraulic mounts of an off-road vibratory roller. *Shock Vib* 2019:1–15. <https://doi.org/10.1155/2019/8725382>
- Hua W, Hua X et al (2021) Experimental investigation and vibration control of semi-active hydraulic-pneumatic mounts for vibratory roller cab. *SAE Int J Veh Dyn Stab NVH* 5(4):381–392. <https://doi.org/10.4271/03-15-03-0019>
- International Organization for Standardization (1997) ISO 2631–1 Mechanical vibration and shock—evaluation of human exposure to whole body vibration—Part 2: general requirement. Geneva, Switzerland: International Organization for Standardization
- Fargione G, Tringali D, Risitano G (2016) A fuzzy-genetic control system in the ABS for the control of semi-active vehicle suspensions. *Mechatronics* 39:89–102. <https://doi.org/10.1016/j.mechatronics.2016.08.004>
- Robert J, Kumar P, Nair S, Swarneswar B (2022) Fuzzy control of active suspension system based on quarter car model. *Mater Today Proc* 66:902–908. <https://doi.org/10.1016/j.matpr.2022.04.575>
- Nguyen V, Jiao R, Zhang J (2020) Control performance of damping and air spring of heavy truck air suspension system with optimal fuzzy control. *SAE Int J Veh Dyn Stab NVH* 4(2):179–194. <https://doi.org/10.4271/10-04-02-0013>
- Homaeinezhad MR, Gavari MA (2022) Feedback control of actuation-constrained moving structure carrying Timoshenko beam. *Int J Robust Nonlinear Control*. <https://doi.org/10.1002/rnc.6471>
- Ebrahimi N, Gharaveisi A (2012) Optimal fuzzy supervisor controller for an active suspension system. *Int J Soft Com Eng* 2(4):36–39
- Li S, Jiao R, Ni D, Zhou H et al (2022) Isolation efficiency of vehicle seat suspension with three quasi-zero stiffness models. *Int J Acoust Vib* 27(3):210–220. <https://doi.org/10.20855/ijav.2022.27.31858>
- Ni D et al (2022) Performance analysis of the seat suspension using different models of the optimal negative-stiffness-structures. *Proc IMechE Part D J Automob Eng* 237:1–12. <https://doi.org/10.1177/09544070221091040>
- Zha J, Ni D, Su B et al (2022) Optimizing the geometrical dimensions of the seat suspension equipped with a negative stiffness structure based on a genetic algorithm. *SAE Int J Veh Dyna Stab NVH* 6:11–20. <https://doi.org/10.4271/10-06-02-0010>
- Chang Y, Zhou J, Wang K, Xu D (2022) Theoretical and experimental investigations on semi-active quasi-zero-stiffness dynamic vibration absorber. *Int J Mech Sci* 214(15):106892. <https://doi.org/10.1016/j.ijmecsci.2021.106892>
- Zhang X (2013) Modelling, simulation and optimization of ride comfort for off road articulated dump trucks. Southeast University, Nanjing
- Bekker M (1969) Introduction to terrain-vehicle system. University of Michigan Press, Ann Arbor, USA
- International Organization for Standardization (1982) ISO/TC108/SC2/WG4 N57 Reporting vehicle road surface irregularities. Stuttgart, Germany: Thieme Medical, Publishers
- Wong J (2001) Theory of ground vehicles. John Wiley & Sons, New York, NY, USA
- Mitschke M (1972) Dynamik der kraftfahrzeuge. Berlin, Springer-Verlag, Berlin. <https://doi.org/10.1007/978-3-662-11585-5>
- Mamdani E, Assilian S (1999) An experiment in linguistic synthesis with a fuzzy logic controller. *Int J Human-Comput Stud* 51:135–147
- Bernadette K, Odon M, Judith W et al (2015) Finite element analysis of vibratory roller response on layered soil systems. *Comput Geotech* 67:73–82. <https://doi.org/10.1016/j.compgeo.2015.02.015>

Springer Nature or its licensor (e.g. a society or other partner) holds exclusive rights to this article under a publishing agreement with the author(s) or other rightsholder(s); author self-archiving of the accepted manuscript version of this article is solely governed by the terms of such publishing agreement and applicable law.